Parametric study of failure mechanisms and optimal configurations of pseudo-ductile thin-ply UD hybrid composites

Meisam Jalalvand *, Gergely Czél, Michael R. Wisnom

Advanced Composites Centre for Innovation and Science, University of Bristol, Bristol BS8 1TR, UK

A B S T R A C T

The effect of different parameters on the gradual failure and pseudo-ductility of thin UD hybrids is studied using an analytical method developed recently. Damage mode maps are proposed to show the effect of different geometric parameters for a specific material combination. This type of map is a novel and efficient method to find the optimum configuration of UD hybrids and also indicates the importance of thin layers to achieve the optimum geometric parameters in practice. The material parametric study reveals that there is always a trade-off between the "yield stress" and the amount of pseudo-ductility; higher yield stresses leads to lower pseudo-ductility and vice versa. However, application of high-stiffness fibres with high strengths as the low strain material can provide both better pseudo-ductility and yield stress.
© 2015 The Authors. Published by Elsevier Ltd. This is an open access article under the CC BY license (http://creativecommons.org/licenses/by/4.0/).

1. Introduction

Conventional composite laminates suffer from sudden brittle failure and large values of safety factor are usually applied in design procedures. Hybridisation is one of the methods for introducing pseudo-ductility to composite materials and avoiding catastrophic failure. By combining different types of *low strain* and *high strain* fibres and selecting an appropriate configuration, it is possible to obtain a gradual failure process and a nonlinear stress–strain response. But if the configuration and material combination is not selected appropriately, not only is the tensile response brittle, but also the mechanical properties of the hybrid are worse than those of the constituents.

Aveston et al. [1–3] investigated the importance of the constituents' proportions and showed that there is an upper limit for the volume ratio of the low strain material to high strain material for avoiding complete fracture at the failure of the low strain material. They concluded that using more low strain material than this critical proportion leads to catastrophic failure whereas lower proportions result in multiple individual cracks along the specimen known as multiple fracture or fragmentation of the low strain material.

Compared to other parameters such as local fibre arrangement studied in [4,5], the proportion of low to high strain material is more important. But, it has been shown [6,7] that it is not possible to achieve fragmentation with thick layers of low strain material,

although the low strain material proportion is lower than the critical value proposed by Aveston et al. It is now clear that the absolute thickness of the constituents plays an important role which was not considered in the model proposed by Aveston et al. [1,2]. Czél and Wisnom [6] showed that hybrid specimens with the same low to high strain material thickness ratio but different ply thicknesses have significantly different stress–strain curves due to their different susceptibility to delamination.

A new analytical approach for predicting all possible damage modes of thin-ply UD hybrids has recently been proposed [8]. This method considers the three different damage modes of (i) low strain material failure/fragmentation, (ii) delamination, and (iii) high strain material failure. The required stress for each damage mode is calculated separately and the stress–strain response of the hybrid is predicted on the basis of these stresses and the order of the damage modes.

The tensile response of thin-ply UD hybrids is affected simultaneously by two groups of geometric and material parameters. The aim of this paper is to investigate the effect of both groups using the analytical approach proposed in [8] with all of the possible damage modes taken into account. Some specific material combinations such as Kevlar/carbon [9], glass/carbon [10] and high strength/high modulus carbon [11] have been studied experimentally but the design procedure including selection of configuration and material combination was judicious. The main aim of this study is to provide a coherent parametric study which takes both geometric and material parameters into account.

The effect of the configuration parameters (proportion and absolute thickness of constituents) is investigated by means of

---

* Corresponding author.
  E-mail address: m.jalalvand@bristol.ac.uk (M. Jalalvand).

novel *Damage Mode Maps* which were presented conceptually in [7]. Here, the approach is developed more thoroughly and the maps are drawn precisely with calculated boundaries between the different regions.

It is not straightforward to use numerical methods such as [7] for parametric studies, especially when the number of material properties affecting the results is high. However the analytical method [8] is an ideal way to investigate the effect of material selection on the hybrid's tensile behaviour. The parametric study in this way will be done in the framework of analytical equations so it is fast to perform and provides a full set of required results easily.

1.1. Pseudo-ductility and yield stress

When damage initiates and develops gradually in a hybrid specimen, the stress–strain response deviates from the initial linear elastic straight line. Fig. 1(a and b) shows two types of generalised nonlinear tensile responses. The two important features of a nonlinear stress–strain curve are (i) the extra strain obtained due to gradual failure called "pseudo-ductile" strain and (ii) the stress level at which the tensile response deviates from the initial linear elastic behaviour, referred to as "yield stress".

A unified and clear definition of pseudo-ductility and yield stress is necessary to compare different types of nonlinear tensile stress–strain response. The pseudo-ductile strain (ϵ_d) is defined here as the extra strain between the final failure point and the initial slope line at the failure stress level as shown in Fig. 1(a). If the stress–strain response includes loss of integrity such as long interlaminar cracks before final failure, the pseudo-ductile strain is measured from that point. Therefore, the pseudo-ductile strain is taken as zero (brittle failure) if the load drop occurs as the first initial nonlinearity in the stress–strain response, as shown in Fig. 1(b).

The yield stress (σ_Y) of a nonlinear tensile response is associated with the knee point where the tensile response deviates from the initial linear elastic line and it is shown in Fig. 1(a). It is worth mentioning that the term "yield stress" is used here to refer to the knee point where the stress–strain curve deviates from the initial elastic line and does not necessarily indicate the presence of plastic deformation in the hybrid laminates as was discussed in [12] for discontinuous carbon/continuous glass hybrid composite.

2. Damage mode map

The inevitable first damage mode in any UD hybrid composite is the failure of the low strain material but the following damage mode depends on the constituents' configuration and material properties. Table 1 summarises the three stress levels of (i) fragmentation in the low strain material, $\sigma_{@LF}$, (ii) delamination,

Table 1
Stress at laminate level for each damage mode [8].

Damage mode	Criterion
Fragmentation in the low strain material	$\sigma_{@LF} = S_L \dfrac{\alpha\beta + 1}{\alpha(\beta + 1)}$
Delamination	$\sigma_{@del} = \dfrac{1}{1+\beta}\sqrt{\left(\dfrac{1+\alpha\beta}{\alpha\beta}\right)\left(\dfrac{2G_{IIC}E_H}{t_H}\right)}$
Failure of the high strain material	$\sigma_{@HF} = \dfrac{1}{(1+\beta)}\dfrac{S_H}{K_t \sqrt[m]{V}}$

$\sigma_{@del}$, and (iii) high strain material failure, $\sigma_{@HF}$ The value of required stress for fragmentation in the low strain material, $\sigma_{@LF}$, is based on assuming an undamaged specimen but for the delamination stress, $\sigma_{@del}$, the low strain material is assumed to be cracked. Since high strain material failure occurs after either low strain material failure or delamination, $\sigma_{@HF}$ is calculated based on assuming a damaged specimen. The details of the analytical approach were fully discussed in [8]. S_L and S_H are the reference strengths of the low and high strain materials and G_{IIC} is the mode II interlaminar fracture toughness. E and t are used for the fibre direction modulus and thickness of the High and Low strain materials specified by H and L indices. α and β are the modulus and thickness ratios of the low to high strain materials. V and m are the volume and Weibull strength distribution modulus of the high strain material and K_t is the stress concentration factor in the high strain material. Details of the derivation of the equations can be found in [8]. It is worth noting that t_L and t_H are the half thicknesses of the low and high strain materials.

The three damage modes compete with each other and whichever has a lower stress requirement, takes place before the other two. For any hybrid configuration, it is possible to calculate the values of stress for fragmentation in the low strain material ($\sigma_{@LF}$), delamination ($\sigma_{@del}$) and failure of the high strain material ($\sigma_{@HF}$) and then to find out the order of expected damage modes based on the order of the required stresses. The six possible permutations of different damage mode orders are given in Table 2.

In the obtained order, the damage modes occurring after high strain material failure do not take place in reality because the whole specimen fails at this point and high strain material failure is always the final damage mode. Furthermore, if the delamination stress is lower than the low strain material fragmentation stress, there is no chance for fragmentation because the low strain material has already separated from the high strain material. However, the predicted failure stress for high strain material remains valid. Taking account of these points, it is possible to predict the damage process of any UD hybrid laminate as shown in Table 2.

Since the expected damage processes of some cases in Table 2 are similar, the six different permutations are re-cast into four groups: (1) failure of the high strain material, (2) catastrophic
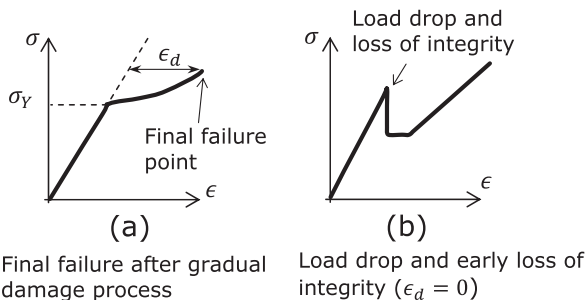
Table 2
Summary of expected damage modes for different conditions after the first crack in the low strain material.

No.	Order of required stress for damage modes	Expected damage process after the initial crack in the low strain material
1a	$\sigma_{@HF} < \sigma_{@LF} < \sigma_{@del}$	1. Failure in the high strain material
1b	$\sigma_{@HF} < \sigma_{@del} < \sigma_{@LF}$	1. Failure in the high strain material
2a	$\sigma_{@del} < \sigma_{@LF} < \sigma_{@HF}$	1. Catastrophic delamination 2. Failure in the high strain material
2b	$\sigma_{@del} < \sigma_{@HF} < \sigma_{@LF}$	1. Catastrophic delamination 2. Failure in the high strain material
3	$\sigma_{@LF} < \sigma_{@HF} < \sigma_{@del}$	1. Fragmentation of the low strain material 2. Failure in the high strain material
4	$\sigma_{@LF} < \sigma_{@del} < \sigma_{@HF}$	1. Fragmentation in the low strain material 2. Dispersed delamination 3. Failure of the high strain material

Fig. 1. (a) A nonlinear stress–strain curve with gradual damage process and (b) a nonlinear stress–strain curve with loss of integrity and load drop before final failure process.

delamination and failure of the high strain material, (3) fragmentation in the low strain material and failure of the high strain material, and (4) fragmentation in the low strain material followed by dispersed delamination and finally failure in the high strain material.

For a specific material combination, the damage process depends only on the laminate configuration i.e. the thickness of the low and high strain materials. Damage mode maps are a good way of visualising this dependency. Using such a map, it is possible to predict the damage process of any UD hybrid composite straightaway.

The damage mode map introduced in [7] was only drawn schematically, using many separate FE analyses with different configurations. FE analysis of each configuration was time consuming and did not result in an accurate boundary between the different damage modes.

In this paper, the damage mode map is drawn precisely, based on the analytical method presented in [8]. The boundaries between different zones with different damage scenarios can be determined precisely by equating any two criteria in Table 1 as discussed later in this section. The whole analysis is analytical and computationally very low-cost.

The configuration of each hybrid can be determined by two independent parameters. The two selected parameters for drawing the damage mode map are the relative thickness and absolute thickness of the low strain material and they are attributed to the horizontal and vertical axes of the damage mode map respectively. The relative low strain material thickness, γ, is defined in the following equation.

$$\gamma = \frac{t_L}{t_L + t_H} = \frac{\beta}{1 + \beta} \tag{1}$$

2.1. Boundary line between fragmentation in the low strain material and delamination

To find out the configurations at which fragmentation in the low strain material initiates before delamination ($\sigma_{@LF} < \sigma_{@del}$), the following inequality should be satisfied.

$$S_L \frac{\alpha\beta + 1}{\alpha(\beta + 1)} < \frac{1}{1 + \beta} \sqrt{\left(\frac{1 + \alpha\beta}{\alpha\beta}\right)\left(\frac{2G_{IIC}E_H}{t_H}\right)} \tag{2}$$

Keeping the material and interface properties constant and using Eq. (1), it is possible to find configurations in which fragmentation initiates before delamination, Eq. (3).

$$t_L < \frac{2G_{IIC}E_H}{S_L^2} \frac{\alpha(1 - \gamma)}{(\alpha\gamma + 1 - \gamma)} \tag{3}$$

2.2. Boundary line between fragmentation in the low strain material and high strain material failure

If the proportion of the low strain material is very high, it is intuitive that after the first crack in the low strain material, the high strain material cannot carry the extra load shed by the broken low strain material layer and fails. To find configurations in which low strain material fragmentation takes place before failure in the high strain material, it is necessary to satisfy $\sigma_{@LF} < \sigma_{@HF}$. Substituting $t_H = t_L/\beta$ into each equation leads to the following equation between low strain material thickness, t_L, and β:

$$\sqrt[m]{t_L} < \frac{S_H}{K_t S_L} \left(\frac{\alpha}{\alpha\beta + 1}\right) \sqrt[m]{\frac{\beta}{2WL}} \tag{4}$$

Eqs. (1) and (4) can be used together in an implicit way to find the relation between absolute and relative thickness of the low strain material, $2t_L$ and γ.

2.3. Boundary line between delamination and high strain material failure

If the delamination stress is lower than the high strain material failure stress, $\sigma_{@del} < \sigma_{@HF}$, delamination propagation is expected before final failure. According to Table 1 and after rewriting the equation for the low strain material thickness, this criterion becomes as in Eq. (5).

$$\beta^{\left(-\frac{1}{m}\right)} \frac{K_t}{S_H} \sqrt[m]{2LW} \sqrt{2G_{IIC}E_H} \sqrt{\frac{1 + \alpha\beta}{\alpha}} < t_L^{\left(\frac{1}{2} - \frac{1}{m}\right)} \tag{5}$$

This equation can be used along with Eq. (1) to draw the boundary between the delamination and high strain material failure.

2.4. Damage mode map of E-glass/TR30 carbon hybrid

Six different layups/configurations made out of E-glass epoxy/TR30 carbon epoxy hybrid have been tested previously [6,7] to cover different possible damage scenarios. The tensile response of these layups has also been analysed with FE [7] and the analytical [8] method. In this section, the damage mode map of E-glass epoxy/TR30 carbon epoxy hybrid is produced.

The carbon layer is the low strain material and the glass layer has the high strain material role. The material properties of the constituents are given in Table 3 [7,8,13,14]. The interlaminar toughness and stress concentration factor have been assumed to be G_{IIC} = 1.0 N/mm and K_t = 1.08. More details can be found in [8].

Fig. 2 shows the six regions of the cases discussed earlier and summarised in Table 2. These regions are divided by the three boundaries given in Eqs. (3)–(5).

Fig. 3 is the damage mode map of E-glass/TR30 carbon hybrid at a new scale and showing the experimental results and previous FE analysis. In [7] different hybrid configurations with the same E-glass/TR30 carbon material combination were analysed using cohesive elements and FE approach. Based on the obtained numerical results, the configurations were categorised into four different groups. Fig. 3 shows the different tested and analysed configurations with the boundaries found from Eqs. (3)–(5). Consistent with the FE analysis, the boundaries between regions 1a and 1b as well as regions 2a and 2b are not drawn since these regions have similar damage scenarios.

The square markers highlight the tested specimens of [EG/C_m/EG] and [EG_2/C_n/EG_2] (m = 1, 2 and n = 1–4) in [6,7] where EG and C stand for E-glass and TR30 carbon layers. All of the simulated models with similar damage scenarios are highlighted with the same marker style. The two regions for cases 1a and 1b as well as 2a and 2b of Table 2 have not been separated since the resulting failure modes are identical. The boundaries successfully separate each group of laminates which have similar damage processes and the damage mode map matches very well with the observed damage scenarios in the experimental and FE results. The [EG_2/C_2/EG_2] laminate is very close to the border line between the

Table 3
Material properties of E-glass, S-glass and TR30 carbon composites.

	E_1 (GPa)	Ref. strength (MPa)	Ply thickness (mm)	Weibull modulus
Hexcel E-Glass/913 [14]	38.7[a]	1548[b]	0.144	29.3
Hexcel S-Glass/913 [8]	45.7	2138[b]	0.155	29.3[c]
SkyFlex TR30 carbon epoxy [7,13]	101.7	1962	0.030	–

[a] E_1 = 43.9 GPa for 0.127 mm nominal ply thickness. It is corrected for the measured ply thickness reflecting the lower fibre volume fraction.
[b] Calculated reference strength for unit volume.
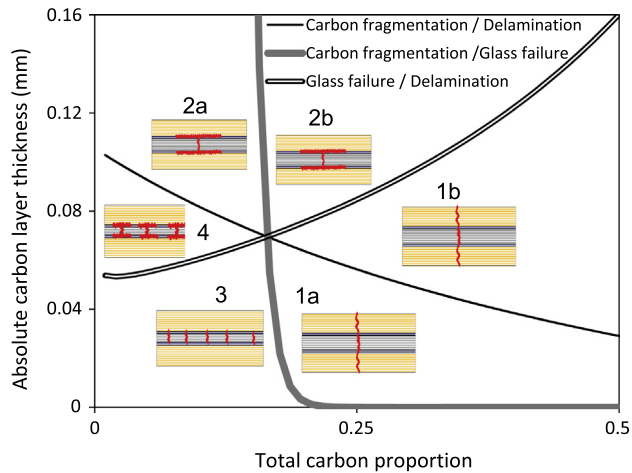[c] Assumed to be equal to the Weibull modulus of E-glass/913 from [13].

Fig. 2. Damage mode map of E-glass/TR30 carbon hybrid. (For interpretation of the references to colour in this figure legend, the reader is referred to the web version of this article.)

regions for fragmentation only and fragmentation accompanied by diffuse delamination. This suggests that the damage process of this layup is quite sensitive to the material and geometric parameters and in the tests was found to be a mixture of both damage scenarios. Such sensitivity has been studied and pointed out in [8] as well. In reality, the border lines of the damage mode map have a width which depends on the variability of the constituents. So the damage process of configurations close to the border lines may be a mixture of the damage scenarios of the adjacent regions.

2.5. Damage mode map of S-glass/TR30 carbon hybrid

The damage mode map of E-glass/TR30 carbon shows that the maximum proportion of carbon to get fragmentation and dispersed delamination in the damage scenario is only about 16%. Due to variability in the constituents and limitation in the minimum ply-thickness, the best layup in that series of experimental tests was [EG$_2$/C$_2$/EG$_2$] with less than 10% total carbon proportion. Since the low strain material content was low, the final pseudo-ductility of this test series was not very high.

To improve the obtained pseudo-ductile strain, a higher strain material is required to replace E-glass/epoxy and S-glass is
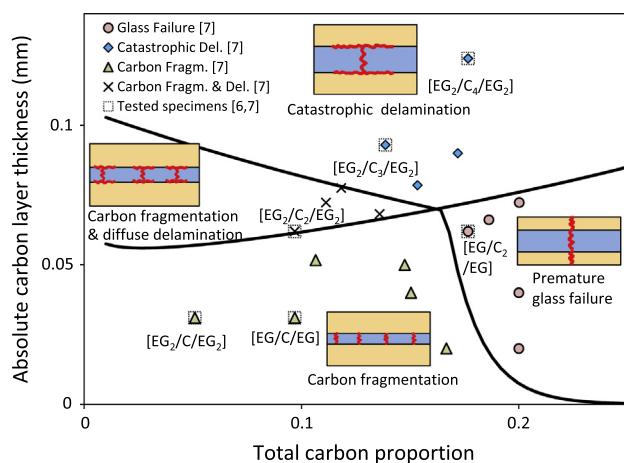

Fig. 3. Comparing the predicted damage mode map of E-glass/TR30 carbon with the results of tested [6] and FE (numerically) modelled [7] laminates – each marker is associated with a case study and full lines are based on Eqs. (3)–(5). (For interpretation of the references to colour in this figure legend, the reader is referred to the web version of this article.)

a suitable material with properties shown in Table 3. The damage mode map of S-glass/TR30 carbon hybrid in Fig. 4 indicates that the total carbon proportion in this hybrid can be increased up to about 27%, so better results can be expected from this material combination.

Using the definition given in the introduction, it is possible to plot the distribution of pseudo-ductile strain and yield stress on the damage mode map for the regions where the failure process is gradual (regions 3 and 4 of Table 2). The distribution of pseudo-ductile strain and yield stress for the S-glass/TR30 carbon hybrid is added to the basic damage mode map in Fig. 4. The tested laminates presented in [8], [SG/C$_n$/SG] (n = 1–3) and [SG$_2$/C$_4$/SG$_2$], are shown with circle markers on the map (SG stands for S-Glass). Since the damage process of the [SG/C$_3$/SG] and [SG$_2$/C$_4$/SG$_2$] laminates includes a catastrophic delamination right after the first fragmentation in the carbon layer, there is no pseudo-ductility – these layups are in the delamination region with no pseudo-ductile strain or yield stress. But the pseudo-ductile strain of the [SG/C/SG] and [SG/C$_2$/SG] are about 0.35% and 1.0% which is very close to the experimental and analytical results published in [8].

The yield stresses of these two layups from Fig. 4(b) are about 950 MPa and 1060 MPa but the experimental results are 1170 MPa and 1130 MPa. The main reason for the difference between the damage mode map prediction and experimental results is that the materials are assumed to be ideal without any variability in the strength. However, the average strength of different points in the carbon layer is higher than the minimum strength value and the deviation from the initial straight line of the stress–strain curve occurs at higher strains.

Additionally, the [SG/C/SG] laminate yield stress is predicted to be lower than [SG/C$_2$/SG] but the obtained experimental values are the opposite way round. This is because the thickness of the [SG/C/SG] laminate is half of the [SG/C$_2$/SG] laminate and its fragmentation density (number of cracks in the carbon per unit length) is double. Therefore more cracks are required for deviation of the stress–strain curve from the initial linear elastic line. Due to the variability in the material strength, the larger number of cracks results in a higher value of yield stress in the [SG/C/SG] laminate.

Fig. 4 clearly shows that the highest value of pseudo-ductile strain can be achieved with configurations very close to the intersection of all three boundary lines in region number 4 (see Table 2).

3. Material parametric study

One of the main advantages of using an analytical method for the parametric study is that it can be done within the framework of formulae and equations, so it is very quick and straightforward. In this section, the dependency of different characteristics of the hybrid stress–strain response such as pseudo-ductile strain, yield stress and strength of the hybrid on the constituent material properties is investigated. The main outcome is a better understanding of the potential of the hybrid materials and guidelines for optimising the material combination.

3.1. Maximum pseudo-ductile strain

According to the damage mode map and the pseudo ductile strain (ϵ_d) contours shown in Fig. 4, the highest value of pseudo-ductile strain can be achieved if the hybrid configuration is within the boundary of region 4 (see Table 2) and close to the apex. This area is at the intersection of the three boundaries between different damage modes. Therefore, the highest theoretical values of pseudo-ductile strain for a specific material combination can be associated with the configuration at the boundaries' intersection point. The results from this configuration with the highest
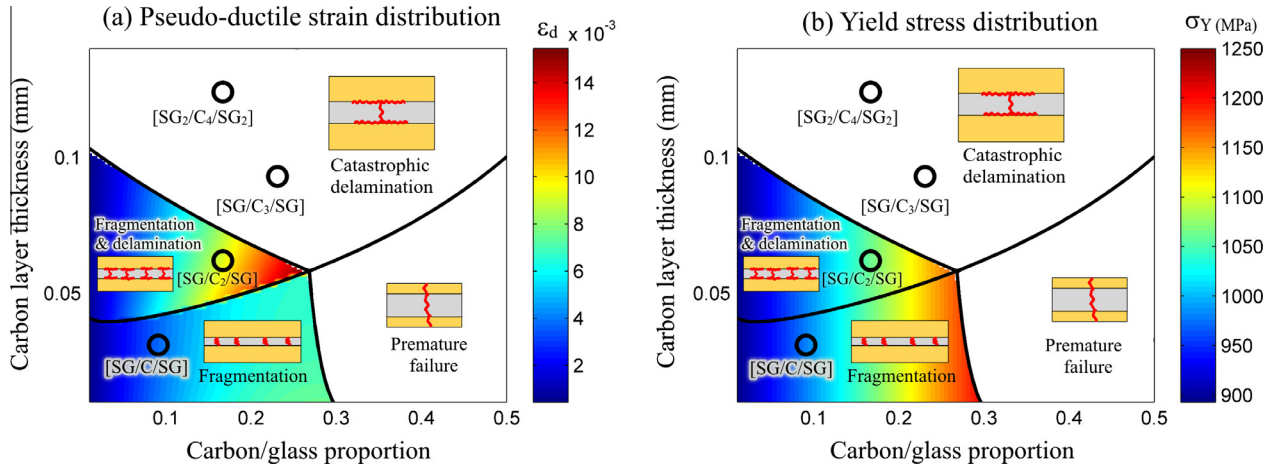
Fig. 4. Distribution of (a) pseudo-ductile strain, ϵ_d, and (b) yield stress, σ_Y, on the damage mode map of S-glass/TR30 carbon hybrid – circles correspond to $[G/C_n/G]$ ($n = 1$–3) and $[G_2/C_4/G_2]$ laminates. (For interpretation of the references to colour in this figure legend, the reader is referred to the web version of this article.)

theoretical pseudo-ductile strain can be assumed as the representative output of that material set. With this assumption, the best results of different material combinations can be compared to each other without the need to present any information on the actual configuration and layer thicknesses.

To find the intersection of the boundaries, it is only necessary to equate any two of the Eqs. (3)–(5). However, this will lead to a non-linear equation which does not have a simple analytical solution. To keep the study quick and simple, the size effect in the high strain material failure is ignored here and Eqs. (4) and (5) are approximated by simpler versions in which, no Weibull Modulus is incorporated. This approximation does not significantly affect the results of material parametric study since the value of Weibull modulus, m, is typically more than 25 and the final outcome of all of the terms with $1/m$ exponent is close to 1. However, this approximation significantly helps to get a much easier and faster solution. Similarly the final outcome of $\sqrt[m]{V}$ for typical values of t_L is close to 1. Therefore, the inequality (4) is more sensitive to the value of β (or γ) rather than t_L. The approximate maximum values of β can be found by replacing $\sqrt[m]{V}$ in the high strain material failure stress (given in Table 1) with 1. This leads to a relation independent of low strain material thickness, Eq. (6).

$$\beta < \frac{S_H}{K_t S_L} - \frac{1}{\alpha} = \frac{S_H}{K_t S_L} - \frac{E_H}{E_L} \qquad (6)$$

Eq. (6) is similar to the load transfer criterion presented in [2,3] by Aveston et al. where no size effect was considered. Similar to the ratio of modulus and thickness of the low and high strain material, it is possible to define the strength ratio as $\lambda = \frac{S_L}{S_H}$. Therefore, Eq. (6) can be rewritten as:

$$\beta < \frac{1}{K_t \lambda} - \frac{1}{\alpha} \qquad (7)$$

It is also possible to neglect the size effect in (5) for the condition of getting delamination before high strain material failure as in (8).

$$\frac{K_t}{S_H} \sqrt{2 G_{IIC} E_H} \sqrt{\frac{1 + \alpha\beta}{\alpha}} < \sqrt{t_L} \qquad (8)$$

The intersection point coordinate (relative and absolute thickness of the low strain material) with highest pseudo-ductile strain can now be found by equating two of the boundary equations from

(3), (6), (8). Since the intersection of all of the three equations is the same, it does not matter which two criteria are selected and the final results will be the same.

Substituting Eq. (6) into (3) and assuming equal strength and strength distribution average for the low strain material ($\acute{S}_L = S_L$), the low strain material to high strain material ratio and the absolute thickness of the low strain material at the intersection is found as in Eqs. (9) and (10).

$$\beta = \frac{1}{K_t \lambda} - \frac{1}{\alpha} \qquad (9)$$

$$t_L = \frac{2 G_{IIC}}{S_L} \frac{K_t}{\epsilon_{HF}} \qquad (10)$$

According to Eq. (9), the thickness ratio of the low strain material to high strain material at the intersection point of the boundaries on the damage mode map is independent of the interlaminar toughness but the absolute thickness of the low strain material at the intersection is proportional to the interlaminar toughness.

At the intersection point, all of the three damage modes occur at the same point. Therefore, the yield stress, strength of the laminate, fragmentation stress, delamination stress and high strain material failure stress, all are equal to each other. In other words, substituting the absolute and relative low strain material thickness from Eqs. (9) and (10) into any of the equations given in Table 1 results in the same maximum yield stress, σ_{Y_max}, as given in Eq. (11). It is worth mentioning that the size effect term ($\sqrt[m]{V}$) is ignored in deriving (11).

$$\sigma_{Y\_max} = \frac{S_L \alpha}{\alpha K_t \lambda + \alpha - K_t \lambda} \qquad (11)$$

The damage initiation strain is equal to the failure strain of the low strain material, ϵ_{FL} and the final failure strain of the laminate is equal to ϵ_{HL}/K_t if the size effect term ($\sqrt[m]{V}$) is ignored, based on the analytical method presented in [8]. The stress–strain response of an arbitrary material combination with the highest theoretical pseudo-ductile strain and the optimum configuration given in Eq. (9) is shown in Fig. 5.

Based on the stress–strain curve shown in Fig. 5, the maximum pseudo-ductile strain of any material combinations is given by (12).

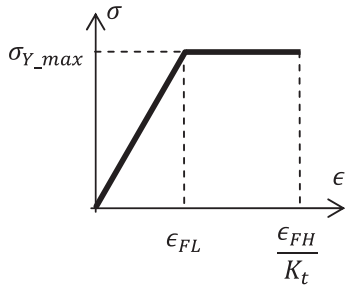$$\epsilon_{d\_max} = \frac{\epsilon_{FH}}{K_t} - \epsilon_{FL} \qquad (12)$$

Fig. 5. Theoretical stress–strain curve of a UD hybrid material combination with maximum theoretical pseudo-ductile strain.

Eqs. (11) and (12) show that the yield stress and pseudo-ductile strain of an ideal UD hybrid material only depend on the mechanical properties of the constituent layers and not on the interface properties. The interface toughness only affects the optimum absolute thickness of the constituent layers. Eq. (10) also shows that the ratio of the optimum thickness of the low strain material and the interlaminar toughness is constant for a specific hybrid combination. So the optimum thickness of the low strain material is proportional to the interlaminar toughness if the constituents are kept the same.

If the value of stress concentration in Eq. (12) is assumed to be equal to one ($K_t = 1$) rather than 1.08, the maximum pseudo-ductile strain of a certain material configuration is equal to the difference between the failure strain of the low and high strain materials, provided that the configuration is optimum. In other words, the difference between failure strains of the low and high strain materials is the highest possible pseudo-ductile strain that can be achieved for a UD hybrid composite.

3.2. Low and high strain material with similar moduli

As shown in the previous section, the pseudo-ductile strain and yield stress of UD hybrid composites are functions of the constituents' material properties. Let's assume that the low and high strain material have the same moduli ($E_L = E_H$ or $\alpha = 1$). Since the pseudo-ductile strain of the optimum configuration does not depend on the modulus of the constituents, Eq. (12) does not change, but the maximum yield stress of such a combination after simplifying Eq. (11) becomes equal to the low strain material strength, $\sigma_{Y\_max} = S_L$. Fig. 6(a) shows the stress–strain response of the low and high strain materials and Fig. 6(b) shows the response of their optimum hybrid combination. The low and high strain materials fail catastrophically at ϵ_{FL} and ϵ_{FH} strain respectively but in the hybrid composite, damage initiates at ϵ_{FL} and continues to develop up to ϵ_{FH}. The yield stress of the hybrid configuration is

equal to the strength of the low strain material which is lower than the strength of the high strain material. But the hybrid's response has an important advantage over the high strain material and that is the pseudo-ductility in this material. This example clearly shows that there is a trade-off between strength/yield stress and pseudo-ductile strain in hybrid materials.

3.3. Parametric study

To study the effect of different material parameters, the pseudo-ductile strain and yield stress values are considered as the two main parameters representing the performance of a UD hybrid composite. To generalise the study and obtain non-dimensional variables, the pseudo-ductile strain and yield stress values are divided by the failure strain and strength of the high strain material respectively. The value of non-dimensional pseudo-ductile strain (ϵ_d/ϵ_{FH}) and yield stress (σ_Y/S_H) can vary between 0 and 1. Fig. 7 shows schematic stress–strain responses of the low and high strain materials as well as the tensile response of their optimum hybrid combination. To study the effect of different material combinations, the high strain material is kept constant and the material properties of the low strain material are changed in different ways. No restriction is applied on the low strain material stress–strain response except to keep its failure strain lower than the failure strain of the high strain material.

In Figs. 8–10, the variation of non-dimensional yield stress (solid lines) and pseudo-ductile strain (dashed lines) for different hybrid combinations is shown on two separate vertical axes on the right and left of the diagram. These figures clearly show that there is a trade-off between yield stress and pseudo-ductile strain.
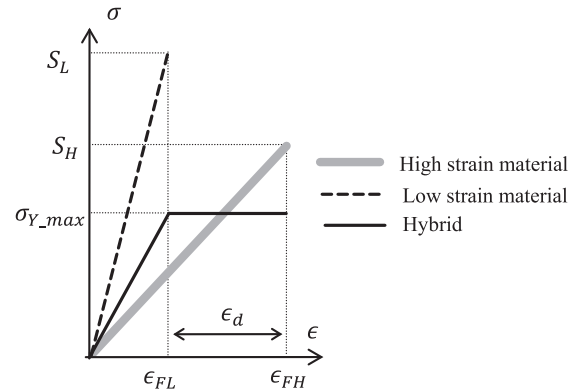

Fig. 7. Stress–strain responses of a low and high strain material and their optimum hybrid layup.

(a) Stress strain response of low and high strain materials with similar moduli

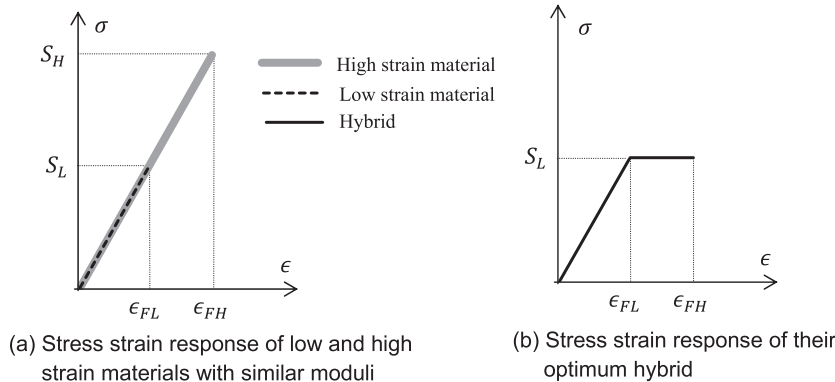(b) Stress strain response of their optimum hybrid

Fig. 6. Stress–strain responses of (a) a low and high strain material and (b) the optimum hybrid layup with similar modulus ($E_L = E_H$ or $\alpha = 1$).

Fig. 8 indicates these two variables versus modulus and strength ratios. Any increase in the modulus ratio (α) leads to an increase in the pseudo-ductile strain and a simultaneous decrease in yield stress values. Increasing the strength ratio (λ) is the opposite, resulting in higher values of yield stress and reduction in pseudo-ductile strains.

The intersections of the dashed and solid lines with the same colour are hybrid laminates with equal non-dimensional yield stress and pseudo-ductile strain and are shown by circular markers in Fig. 8. For strength ratio $\lambda = S_L/S_H = 0.5$, it is possible to make a hybrid with non-dimensional yield stress and pseudo-ductile strain both of 0.5. A strength ratio of $\lambda = 2.0$ leads to a hybrid with 0.73 non-dimensional yield-stress and pseudo-ductile strain. This shows that increasing the strength ratio makes a better overall compromise, if the stiffness ratio is increased accordingly.

Fig. 9 indicates the variation of non-dimensional yield stress and pseudo-ductile strain for different failure strain (η) and strength (λ) ratios. The yield stress curves are ascending and pseudo-ductile strain curves are descending which is similar to the compromise shown in Fig. 8. However, the non-dimensional pseudo-ductile strain curves are independent of strength ratios and are all coincident. Therefore, it is obvious that larger strength
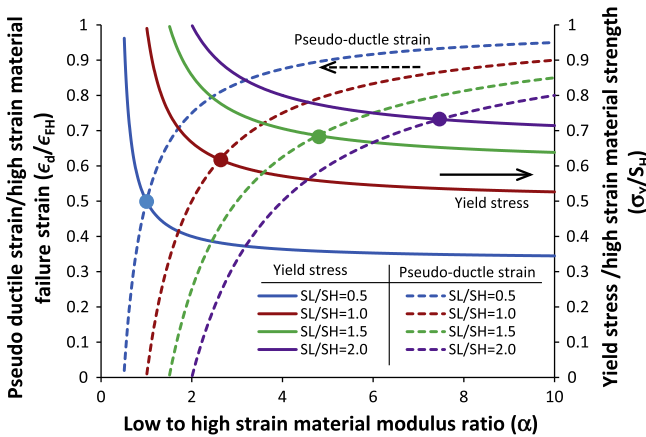

Fig. 10. Non-dimensional yield stress and pseudo-ductile strain values for different stiffness ratios E_L/E_H (α) and failure strain ratios (η). (For interpretation of the references to colour in this figure legend, the reader is referred to the web version of this article.)
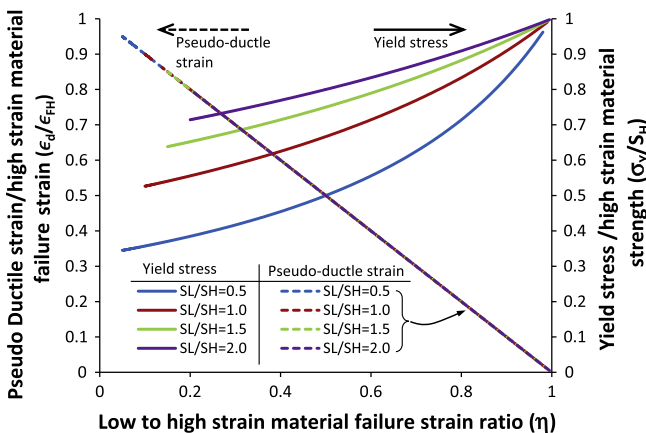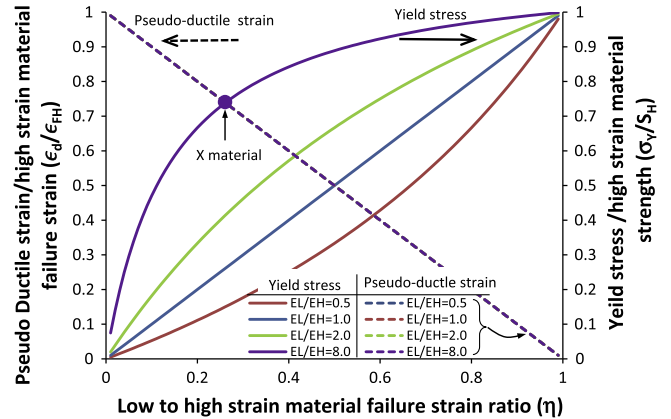
ratios give higher yield stresses and makes a better overall trade-off between yield stress and pseudo-ductile strain.

Fig. 10 shows the non-dimensional yield stress and pseudo-ductile strain variation for different failure strain and elastic modulus ratios to study the importance of the Young's modulus ratio. Similar to Fig. 9, the horizontal axis is the failure strain ratio (η) but each curve is for a constant stiffness ratio. Since the pseudo-ductile strain is only dependent on the failure strains of the low and high strain material, all of the results for various strength ratios are coincident on a straight line. All yield stress curves intersect each other at failure strains ratios of 0 and 1. This means that regardless of the stiffness values, application of a low strain material with a failure strain equal to the failure strain of the high strain material results in a hybrid with zero pseudo-ductility which fails catastrophically. Comparing low strain materials with similar failure strains but different moduli, the pseudo-ductile strain is similar but those with higher stiffness have higher yield stresses.

Both Figs. 9 and 10 show that with stronger and stiffer low strain material, it is possible to achieve better pseudo-ductile strains and yield stresses.

4. Discussion

In this paper, the analytical method proposed for UD hybrid damage analysis [8] was applied to study the effect of different geometric and material parameters.

Damage mode maps have been proposed to study the effect of the hybrid configuration on the damage process. This approach visualises the effect of different geometric parameters on the stress–strain curve of the hybrid and its characteristic parameters such as pseudo-ductile strain and yield stress. Therefore, it has been found to be a very useful tool for designing hybrid configurations with specific material combinations. It has also been shown that the highest value of pseudo-ductile strain can be achieved if all damage modes in the hybrid specimen (low strain material fragmentation, dispersed delamination and high strain material failure) occur at stress levels close to each other. Configurations very close to the intersection of the boundaries of damage mode map in region 4 (see Table 2) on the damage mode map satisfy this condition.

The configuration associated with the intersection of the boundaries of the damage mode map can represent the maximum theoretical pseudo-ductile strain of each material combination. The highest theoretical pseudo-ductile strain and yield stress values only depend on the mechanical properties of the constituents

Fig. 8. Non-dimensional yield stress and pseudo-ductile strain values for different stiffness ratios (α) and strength ratios S_L/S_H (λ). (For interpretation of the references to colour in this figure legend, the reader is referred to the web version of this article.)

Fig. 9. Non-dimensional yield stress and pseudo-ductile strain values for different strength ratios S_L/S_H (λ) and failure strain ratios (η). (For interpretation of the references to colour in this figure legend, the reader is referred to the web version of this article.)

and are independent of the interface properties, but the shape of the damage mode map and the absolute thickness of the constituents depend on all material properties including interface toughness. The damage mode map of S-glass/TR30 carbon hybrid with an interfacial toughness of G_{IIC} = 2.0 N/mm (twice the actual toughness) is shown in Fig. 11. The maximum value of pseudo-ductile strain and yield stress is the same as the damage mode map shown in Fig. 4 but the areas with gradual failure (coloured areas on the map) are expanded vertically and achieving the optimum configuration is significantly easier in practice. All four tested layups discussed in Section 2.5 and Fig. 4 now give a gradual failure process and the best one in terms of pseudo-ductile strain is [SG$_2$/C$_4$/SG$_2$]. The carbon layer thickness for this layup is double the optimum layup with G_{IIC} = 1 N/mm so less thin ply layers can be used for producing pseudo-ductile hybrids if the interlaminar toughness is increased. The damage mode map is compressed vertically if the value of interlaminar toughness is decreased and therefore, thinner carbon layers which are harder to manufacture are required for an optimal configuration.

To study the effect of different material combinations on the stress–strain response, the pseudo-ductile strain and yield stress of different material combinations with their optimum configurations have been investigated in the material parametric study

section. It was shown that there is always a trade-off between the pseudo-ductile strain and yield stress. The highest possible pseudo-ductile strain is equal to the difference between the failure strain of the high and low strain materials. This value of pseudo-ductile strain may be achieved if the configuration is optimum and the stress concentration around the cracks is suppressed.

It was also shown that the overall trade-off between pseudo-ductile strain and yield stress can be improved if high-stiffness low strain materials with relatively low failure strain values are applied. For example, a low strain material with 8 times higher stiffness than the high strain material can give better yield stresses compared to another low strain material with a modulus ratio of 2. If the failure strains of these two candidates for the low strain material are equal, the stiffer one produces a higher yield stress although its pseudo-ductile strain is still equal to the other one.

To improve both pseudo-ductile strain and yield stress, it is necessary to increase both stiffness and strength ratios. The stiffness and strength ratios of TR30 carbon to S-glass composite are about 2.2 and 0.92. Let's assume that material X is available and that its modulus and strength are 8 and 1.54 times those of the S-glass epoxy layer. This material corresponds to the circular marker shown in Fig. 10. The fibre direction modulus of such a material is 365.6 GPa, the strength is 3290 MPa and the failure strain is
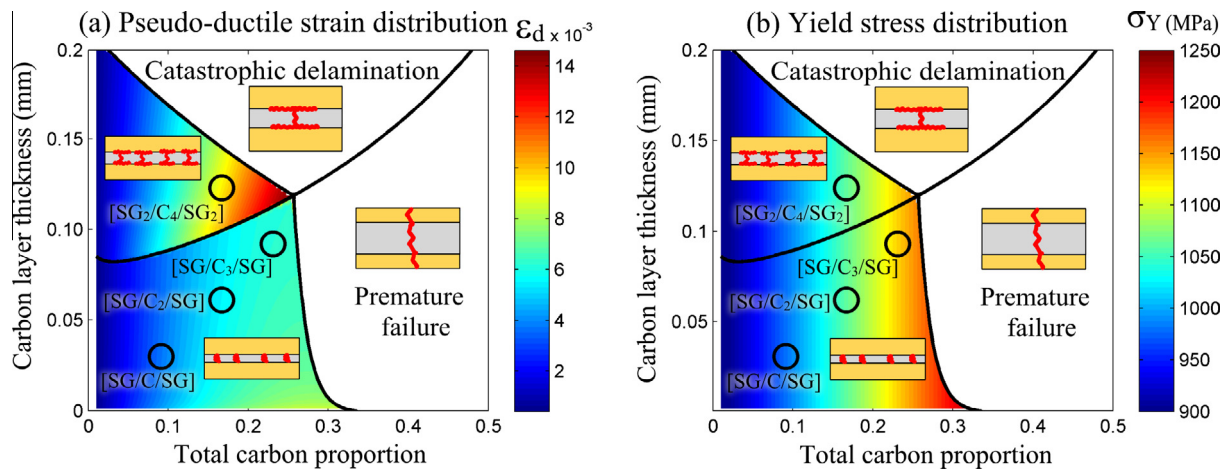

Fig. 11. Damage mode map of S-glass/TR30 carbon hybrid with interlaminar toughness G_{IIC} = 0.5 N/mm and distribution of (a) pseudo-ductile strain, ϵ_d, and (b) yield stress, σ_Y. (For interpretation of the references to colour in this figure legend, the reader is referred to the web version of this article.)
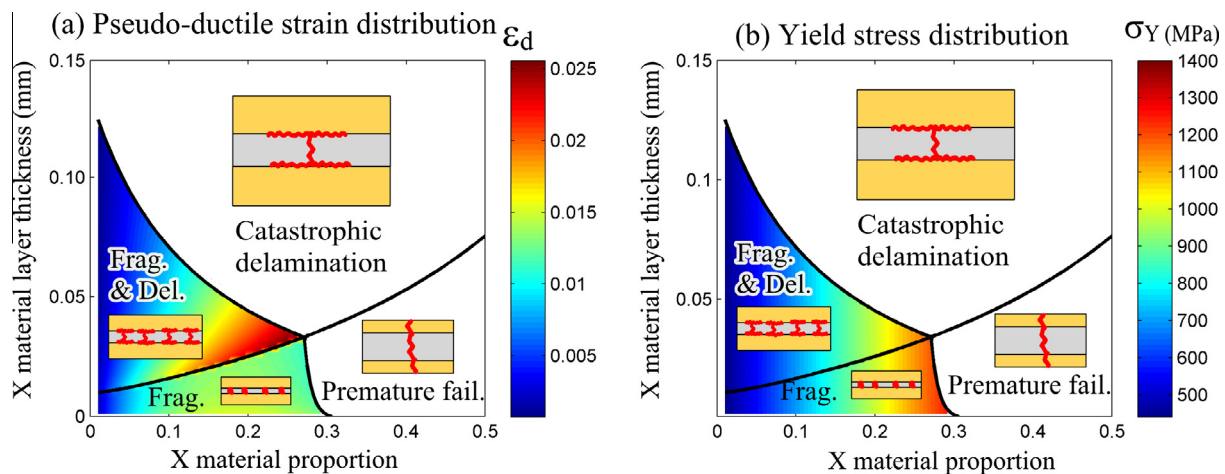

Fig. 12. Damage mode map of S-glass and a material X with 365.6 GPa initial stiffness and 0.9% failure strain along with the distribution of (a) pseudo-ductile strain, ϵ_d, and (b) yield stress, σ_Y. (For interpretation of the references to colour in this figure legend, the reader is referred to the web version of this article.)
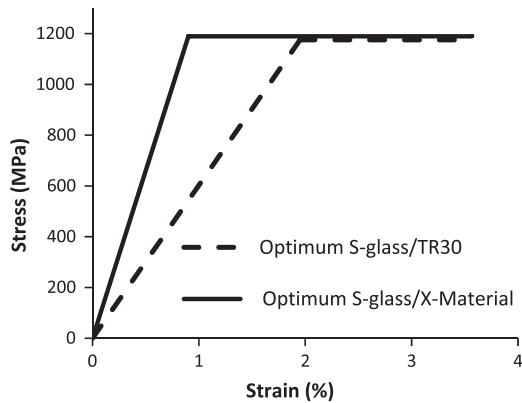
Fig. 13. The tensile response of the optimum hybrid configuration S-glass/TR30 and S-glass/X-material.

about 0.9%. These mechanical properties are not far from those of high modulus carbon fibre composites. For instance, a UD layer of Mitsubishi Rayon HS40 laminates with 60% fibre volume fraction has 274 GPa fibre direction modulus and 2740 MPa strength. Also Toray M55 and Toho Tenax UMS55 fibres with 60% fibre volume fraction give 326 GPa modulus and 2608 MPa strength.

Fig. 12 shows the damage mode map of a hybrid made with this material as the low strain material and S-glass epoxy as the high strain material. The tensile response of the optimum configurations made out of S-glass/TR-30 hybrid is compared against the S-glass/X-material one in Fig. 13. The interfacial toughness is assumed to be 1.0 N/mm. The pseudo-ductile strain, 2.6%, and yield stress, 1200 MPa, are both higher than the maximum values of S-glass/TR30, demonstrating the potential of what could be achieved with optimal combinations of materials. The reason is that the assumed low strain material has higher stiffness as well as strength.

5. Conclusions

The following concluding points are drawn in this study:

- Damage mode maps bring a new approach for analysis and design of UD hybrid laminates. They are easy to produce and can clearly demonstrate the damage processes of different hybrid configurations.
- The pseudo-ductile strain and yield stress values for different hybrid specimens can be drawn on the damage mode map so the tensile performance of different UD configurations can be analysed very quickly without the need to draw their tensile stress–strain curves.
- For a specific material combination, the highest pseudo-ductile strain can be achieved by configurations at the intersection of

the regions on the damage mode map. The highest theoretical value for pseudo-ductile strain is equal to the difference between the failure strains of the low and high strain materials.
- The highest values of pseudo-ductile strain and yield stress are independent of the interface toughness. But higher values of interfacial toughness allow thicker layers, making it easier to get configurations closer to the optimum.
- The material parametric study showed that if only one of the low strain material stiffness or strength properties is changed, the effect on the pseudo-ductile strain and yield stress values are opposite to each other, showing that there is a trade-off between these two key performance parameters. However, if both the stiffness and strength values of the low strain material are increased, both pseudo-ductile strain and yield stress values can be improved.

References

[1] Aveston J, Cooper GA, Kelly A. Single and multiple fracture. In: The Prop. fibre Compos. Conf. Proceedings, Natl. Phys. Lab., Guilford: IPC Science and Technology Press Ltd; 1971. p. 15–26.
[2] Aveston J, Kelly A. Theory of multiple fracture of fibrous composites. J Mater Sci 1973;8:352–62.
[3] Aveston J, Kelly A. Tensile first cracking strain and strength of hybrid composites and laminates. Philos Trans R Soc A Math Phys Eng Sci 1980;294:519–34.
[4] Jones KD, DiBenedetto AT. Fibre fracture in hybrid composite. Compos Sci Technol 1994;51:53–62.
[5] Pitkethly MJ, Bader MG. Failure modes of hybrid composites consisting of carbon fibre bundles dispersed in a glass fibre epoxy resin matrix. J Phys D Appl Phys 1987;20:315–22.
[6] Czél G, Wisnom MR. Demonstration of pseudo-ductility in high performance glass–epoxy composites by hybridisation with thin-ply carbon prepreg. Compos Part A Appl Sci Manuf 2013;52:23–30.
[7] Jalalvand M, Czél G, Wisnom MR. Numerical modelling of the damage modes in UD thin carbon/glass hybrid laminates. Compos Sci Technol 2014;94:39–47.
[8] Jalalvand M, Czél G, Wisnom MR. Damage analysis of pseudo-ductile thin-ply UD hybrid composites – a new analytical method. Compos Part A Appl Sci Manuf 2015;69:83–93.
[9] Harris HG, Somboonsong W, Ko FK. New ductile hybrid FRP reinforcing bar for concrete structures. J Compos Constr 1998;2:28–37.
[10] Bunsell AR, Harris B. Hybrid carbon and glass fibre composites. Composites 1974;5:157–64.
[11] Wu Z, Shao Y, Iwashita K, Sakamoto K. Strengthening of preloaded RC beams using hybrid carbon sheets. J Compos Constr 2007;11:299–307.
[12] Czél G, Jalalvand M, Wisnom MR. Demonstration of pseudo-ductility in unidirectional hybrid composites made of discontinuous carbon/epoxy and continuous glass/epoxy plies. Compos Part A Appl Sci Manuf 2015.
[13] Fuller JD, Wisnom MR. Pseudo-ductility and damage suppression in thin ply CFRP angle-ply laminates. Compos Part A Appl Sci Manuf 2014;69:64–71.
[14] Hallett SR. Numerical investigation of progressive damage and the effect of layup in notched tensile tests. J Compos Mater 2005;40:1229–45.